Bottom-up Synthesis of N=13 Sulfur-doped Graphene Nanoribbons

Giang D. Nguyen,[†‡] Francesca M. Toma,[±‡] Ting Cao,[†‡] Zahra Pedramrazi,[†] Chen Chen,[±] Daniel J. Rizzo,[†] Trinity Joshi,[†] Christopher Bronner,[†] Yen-Chia Chen,[†] Steven G. Louie,[†#] Felix R. Fischer,[±#*] and Michael F. Crommie[†#*]*

[†]Department of Physics and [±]Department of Chemistry, University of California at Berkeley, Berkeley, California 94720, United States
[#]Materials Sciences Division, Lawrence Berkeley National Laboratory, Berkeley, California 94720, United States
[‡]These authors contributed equally.

ABSTRACT
Substitutional doping of graphene nanoribbons (GNRs) with heteroatoms is a principal strategy to fine-tune the electronic structure of GNRs for future device applications. Here we report the fabrication and nanoscale characterization of atomically-precise N=13 armchair graphene nanoribbons featuring regioregular edge-doping with sulfur atoms (S-13-AGNRs) on a Au(111) surface. Scanning tunneling spectroscopy and first principle calculations reveal modification of the electronic structure of S-13-AGNRs when compared to undoped N=13 AGNRs.

KEYWORDS: graphene nanoribbon; bottom-up synthesis; scanning tunneling microscopy and spectroscopy; sulfur doping; DFT calculation

Graphene nanoribbons (GNRs) are quasi-one-dimensional strips of graphene that exhibit novel electronic and magnetic properties.[1–6] These properties can be tuned by engineering GNR structural parameters such as width[7–9] and edge symmetry.[5,8] Recent advances in bottom-up GNR synthesis have yielded new techniques for modulating GNR width[5,8,10] and for introducing dopant heteroatoms[6,11–13] with atomic precision both along the GNR edge and, more recently, along the backbone.[13,14] Up to now, however, edge-doping in bottom-up fabricated GNRs has exclusively relied on the introduction of nitrogen heteroatoms in the form of pyridine and pyrimidine rings along the edges of chevron GNRs.[6,11,12] In this position the electron lone-pair on the trigonal planar nitrogen atoms is not in conjugation with the GNR aromatic π-system. Rather than significantly affecting the GNR density of states or energy gap, the electronegative N-atoms only induce a rigid shift of the energies of both the valence and conduction bands.[6]

Here we report the bottom-up synthesis and characterization of atomically-precise N=13 armchair graphene nanoribbons (S-13-AGNRs) wherein alternating $(CH)_2$ groups lining the edges of the GNRs have been replaced by sulfur atoms. This alternative edge-doping pattern places one of the lone-pairs (having p-character) on trigonal planar S-atoms in full conjugation with the extended π-system of the 13-AGNR. Molecular precursors for S-13-AGNRs (**1** in Figure 1a) are derived from 10,10'-dibromo-9,9'-bisanthracene and feature (2-phenyl)thiophene substituents. A sub-monolayer of **1** was deposited onto a Au(111) surface under ultrahigh vacuum (UHV). Subsequent heating of the decorated Au(111) surface to 200 °C induces a radical step-growth polymerization to give *poly*-**1**. A second annealing step (400 °C) induces a thermal cyclodehydrogenation to yield fully conjugated S-13-AGNRs. Both scanning tunneling microscopy (STM) and scanning tunneling spectroscopy (STS) were used to investigate the structure and to probe the electronic states of the resulting S-13-AGNRs. STS measurements reveal a LUMO state (lowest unoccupied molecular orbital) for S-13-AGNRs at approximately the same energy as previously recorded for undoped 13-AGNRs. When compared to undoped 13-AGNRs, the density of states (DOS) associated with the LUMO in S-13-AGNR spans a significantly broader energy range. These results are consistent with ab-initio simulations of S-13-AGNRs that indicate a sulfur-induced increase in the energy separation between CB and CB+1 as well as between VB and VB–1 13-AGNR band edges (here CB refers to the conduction band and VB refers to the valance band)

The molecular precursor for S-13-AGNRs **1** (Figure 1a) was synthesized through a Suzuki cross-coupling of 2,2',10,10'-tetrabromo-9,9'-bianthracene (**2**) with two equivalents of (2-(thiophen-2-yl)phenyl)boronic acid (**3**) (see supporting information). Oxidative addition favors the sterically less hindered 2,2'-position in the bisanthracene backbone and yields the desired regioisomer **1** as the major product in 44% yield.

Figure 1b shows an STM image of **1** on Au(111) as deposited. The molecules tend to aggregate into irregular islands along the Au(111) herringbone reconstruction with an average height of 0.5 nm. Annealing the molecule-decorated sample at 200 °C for 20 min induces homolytic cleavage of the labile C–Br bonds in **1** followed by radical step-growth polymerization of the intermediate diradical to give *poly*-**1** (Figure 1a). A representative STM image of a linear chain of *poly*-**1** on Au(111) is depicted in Figure 1c. Analogous to the polymer precursor for undoped 13-AGNRs, *poly*-**1** exhibits a pattern of alternating protrusions associated with the preferred conformation of the (2-phenyl)thiophene substituents on the Au(111) surface (the periodicity of the protrusions is 0.83 ± 0.02 nm with an apparent height of 0.43 ± 0.02 nm).[5,8,13] Further annealing of Au(111) samples at 400 °C for 20 minutes induces a thermal cyclodehydrogenation which converts *poly*-**1** into fully cyclized S-13-AGNRs (Figure 1d). The average height and width of the resulting S-13-AGNRs are 0.23 ± 0.01 nm and 1.9 ± 0.2 nm respectively, and are comparable with the dimensions previously reported for undoped 13-AGNRs (0.21 ± 0.01 nm and 1.9 ± 0.2 nm).[4,8]

Statistical analysis of STM images shows that the average length of S-13-AGNRs obtained by this growth procedure is 5 nm (supporting information). We observe some irregular edge structure in our samples following the final cyclodehydrogenation step (Figure S8). These defects might arise from the additional strain induced along the edges of GNRs by the introduction of 5-membered thiophene rings or by deletion of the thiophene ring through fragmentation of the (2-phenyl)thiophene C–C bond during the thermal annealing at 400 °C.

The local electronic structure of S-13-AGNRs was characterized by recording d*I*/d*V* spectra at various positions above the S-13-AGNR decorated surface. Figure 2 shows typical d*I*/d*V* spectra measured at the center and edges of an S-13-AGNR compared to a reference spectrum measured with the STM tip placed above the bare Au(111) substrate. The Au(111) reference spectrum is dominated by a peak centered at a sample bias of $V = -0.3$ V which drops steeply for $V \leq -0.5$ V. This feature is known to originate from the Au(111) surface state,[15] which has a band edge at 0.5 eV below the Fermi energy E_F (E_F corresponds to $V = 0$). All spectra recorded with the STM tip positioned above S-13-AGNRs show a peak for $V < 0$ that is similar to the peak observed when the tip is held above bare Au(111). This makes it difficult to discern whether this feature (when seen at locations above an S-13-AGNR) is due to the intrinsic S-13-AGNR electronic structure (such as the valence band edge) or is due to the underlying Au(111) surface state. A more unambiguous S-13-AGNR spectral feature is observed at $V = 1.22 \pm 0.23$ V. Here a peak can be seen in the d*I*/d*V* spectra at the S-13-AGNR edges that is not observed at either the S-13-AGNR center or in the Au(111) reference spectrum. This behavior is consistent with the spectral signature of GNR band edge states observed previously for N = 5, N = 7 and N = 13 AGNRs,[4,8,10,16] and is

assigned to the S-13-AGNR conduction band edge. This band edge feature lies at almost the same energy as the undoped 13-AGNR conduction band edge (V = 1.21 ± 0.06 V),[8] but is significantly broadened with a full width at half maximum (FWHM) of ΔE = 0.37 ± 0.2 eV compared to ΔE = 0.19 ± 0.07 eV for the undoped 13-AGNR.

In order to better understand how the electronic properties of 13-AGNRs are affected by substitutional sulfur edge-doping, we performed density functional theory (DFT) calculations within the local density approximation (LDA) for both S-doped (Figure 3a) and undoped (Figure 3b) free-standing 13-AGNRs. Our calculations suggest that incorporation of sulfur atoms into the armchair edges only slightly reduces the bandgap (at the DFT-LDA level) of a pristine 13-AGNR, from 0.90 eV to 0.76 eV. In addition, when referenced to the vacuum potential, the CB minimum and VB maximum of S-13-AGNRs have similar energy alignment compared to pristine 13-AGNRs. This behavior is quite different from the previously studied case of nitrogen edge-doped chevron GNRs, whose band edges undergo a nearly rigid shift of ≈ –0.5 eV compared to undoped chevron GNRs.[6] This difference in behavior for N-doped and S-doped GNRs can be explained by the small difference in electronegativity between sulfur and carbon as compared to the large difference between nitrogen and carbon.[17] Furthermore, the sulfur edge-doping causes a significant increase in the energy difference between the CB and CB+1 band edges, as well as between the VB and VB–1 band edges, when compared with pristine 13-AGNRs (Figure 3). This modification to the electronic structure is due to the strong hybridization of S-dopant orbitals with the aromatic network in S-13-AGNRs (Figure 3c) (due to conjugation of the S lone pair with the π-system).

The calculated band structure of S-13-AGNRs is consistent with the experimentally observed dI/dV spectra of Figure 3d. The experimental conduction band edge of S-13-AGNRs is very closely aligned with the conduction band edge observed for undoped 13-AGNRs (similar to the simulated DOS depicted in Figure 3c). The significant broadening of the experimental LUMO feature for S-13-AGNRs compared to undoped 13-AGNRs is also consistent with the predicted increase in energy separation between the CB and CB+1 band edges for S-13-AGNRs as compared to undoped 13-AGNRs (Figure 3).

In conclusion, we have demonstrated the successful bottom-up synthesis of substitutional sulfur edge-doped 13-AGNRs on Au(111), as well as determination of the effect of sulfur edge-doping on the electronic structure of N=13 AGNRs. Both the theoretically determined and experimentally measured S-13-AGNR electronic structure are consistent with the hybridization of sulfur orbitals with the conjugated π-system of the extended carbon network. This characteristic leads to enhanced energy separation of the CB (VB) and CB+1 (VB-1) band edges but, because sulfur and carbon

electronegativities are similar, the energy alignments of N=13 AGNR bands remain relatively unchanged by sulfur doping.

ASSOCIATED CONTENT

Supporting information

Synthetic procedure and characterization of **1;** STM imaging; computational methods

AUTHOR INFORMATION

Corresponding Authors

*crommie@berkeley.edu
*ffischer@berkeley.edu
*sglouie@berkeley.edu

ACKNOWLEDGMENTS

Research supported by the U.S. Department of Energy (DOE), Office of Science, Basic Energy Sciences (BES), under award no. DE-SC0010409 (design, synthesis, and characterization of molecular building blocks) and Nanomachine Program award no. DE-AC02-05CH11231 (surface reaction characterization), by the Office of Naval Research BRC Program (GNR characterization), by the National Science Foundation (NSF) award no. DMR-1206512 (image analysis), and DMR15-1508412 (development of theory formalism). Computational resources have been provided by the DOE at Lawrence Berkeley National Laboratory's NERSC facility. C.B. acknowledges support through the Fellowship Program of the German National Academy of Sciences Leopoldina under Grant No. LPDS 2014-09. T.J. acknowledges support from NSF Graduate Research Fellowship Program under Grant No. DGE 1106400.

REFERENCES

(1) Son, Y.-W.; Cohen, M. L.; Louie, S. G. Half-Metallic Graphene Nanoribbons. *Nature* **2006**, *444*, 347–349.

(2) Tao, C.; Jiao, L.; Yazyev, O. V.; Chen, Y.-C.; Feng, J.; Zhang, X.; Capaz, R. B.; Tour, J. M.; Zettl, A.; Louie, S. G.; *et al.* Spatially Resolving Edge States of Chiral Graphene Nanoribbons. *Nat. Phys.* **2011**, *7*, 616–620.

(3) Bennett, P. B.; Pedramrazi, Z.; Madani, A.; Chen, Y. C.; De Oteyza, D. G.; Chen, C.; Fischer, F. R.; Crommie, M. F.; Bokor, J. Bottom-up Graphene Nanoribbon Field-Effect Transistors. *Appl. Phys. Lett.* **2013**, *103*.

(4) Chen, Y.-C.; Cao, T.; Chen, C.; Pedramrazi, Z.; Haberer, D.; de Oteyza, D. G.; Fischer, F. R.; Louie, S. G.; Crommie, M. F. Molecular Bandgap Engineering of Bottom-up Synthesized Graphene Nanoribbon Heterojunctions. *Nat. Nanotechnol.* **2015**, *10*, 156–160.

(5) Cai, J.; Ruffieux, P.; Jaafar, R.; Bieri, M.; Braun, T.; Blankenburg, S.; Muoth, M.; Seitsonen, A. P.; Saleh, M.; Feng, X.; *et al.* Atomically Precise Bottom-up Fabrication of Graphene Nanoribbons. *Nature* **2010**, *466*, 470–473.

(6) Cai, J.; Pignedoli, C. A.; Talirz, L.; Ruffieux, P.; Söde, H.; Liang, L.; Meunier, V.; Berger, R.; Li, R.; Feng, X.; *et al.* Graphene Nanoribbon Heterojunctions. *Nat. Nanotechnol.* **2014**, *9*, 896–900.

(7) Han, M.; Özyilmaz, B.; Zhang, Y.; Kim, P. Energy Band-Gap Engineering of Graphene Nanoribbons. *Phys. Rev. Lett.* **2007**, *98*, 206805.

(8) Chen, Y. C.; De Oteyza, D. G.; Pedramrazi, Z.; Chen, C.; Fischer, F. R.; Crommie, M. F. Tuning the Band Gap of Graphene Nanoribbons Synthesized from Molecular Precursors. *ACS Nano* **2013**, *7*, 6123–6128.

(9) Son, Y.-W.; Cohen, M. L.; Louie, S. G. Energy Gaps in Graphene Nanoribbons. *Phys. Rev. Lett.* **2006**, *97*, 216803.

(10) Zhang, H.; Lin, H.; Sun, K.; Chen, L.; Zagranyarski, Y.; Aghdassi, N.; Duhm, S.; Li, Q.; Zhong, D.; Li, Y.; *et al.* On-Surface Synthesis of Rylene-Type Graphene Nanoribbons. *J. Am. Chem. Soc.* **2015**, *137*, 4022-4025.

(11) Bronner, C.; Stremlau, S.; Gille, M.; Braußе, F.; Haase, A.; Hecht, S.; Tegeder, P. Aligning the Band Gap of Graphene Nanoribbons by Monomer Doping. *Angew. Chemie - Int. Ed.* **2013**, *52*, 4422–4425.

(12) Zhang, Y.; Zhang, Y.; Li, G.; Lu, J.; Lin, X.; Du, S.; Berger, R.; Feng, X.; Müllen, K.; Gao, H.-J. Direct Visualization of Atomically Precise Nitrogen-Doped Graphene Nanoribbons. *Appl. Phys. Lett.* **2014**, *105*, 023101.

(13) Cloke, R. R.; Marangoni, T.; Nguyen, G. D.; Joshi, T.; Rizzo, D. J.; Bronner, C.; Cao, T.; Louie, S. G.; Crommie, M. F.; Fischer, F. R. Site-Specific Substitutional Boron Doping of Semiconducting Armchair Graphene Nanoribbons. *J. Am. Chem. Soc.* **2015**, *137*, 8872–8875.

(14) Kawai, S.; Saito, S.; Osumi, S.; Yamaguchi, S.; Foster, A. S.; Spijker, P.; Meyer, E. Atomically Controlled Substitutional Boron-Doping of Graphene Nanoribbons. *Nat. Commun.* **2015**, *6*, 8098.

(15) Chen, W.; Madhavan, V.; Jamneala, T.; Crommie, M. F. Scanning Tunneling Microscopy Observation of an Electronic Superlattice at the Surface of Clean Gold. *Phys. Rev. Lett.* **1998**, *80*, 1469–1472.

(16) Ruffieux, P.; Cai, J.; Plumb, N. C.; Patthey, L.; Prezzi, D.; Ferretti, A.; Molinari, E.; Feng, X.; Müllen, K.; Pignedoli, C. A.; *et al.* Electronic Structure of Atomically Precise Graphene Nanoribbons. *ACS Nano* **2012**, *6*, 6930–6935.

(17) Yang, Z.; Yao, Z.; Li, G.; Fang, G.; Nie, H.; Liu, Z.; Zhou, X.; Chen, X.; Huang, S. Sulfur-Doped Graphene as an Efficient Metal-Free Cathode Catalyst for Oxygen Reduction. *ACS Nano* **2012**, *6*, 205–211.

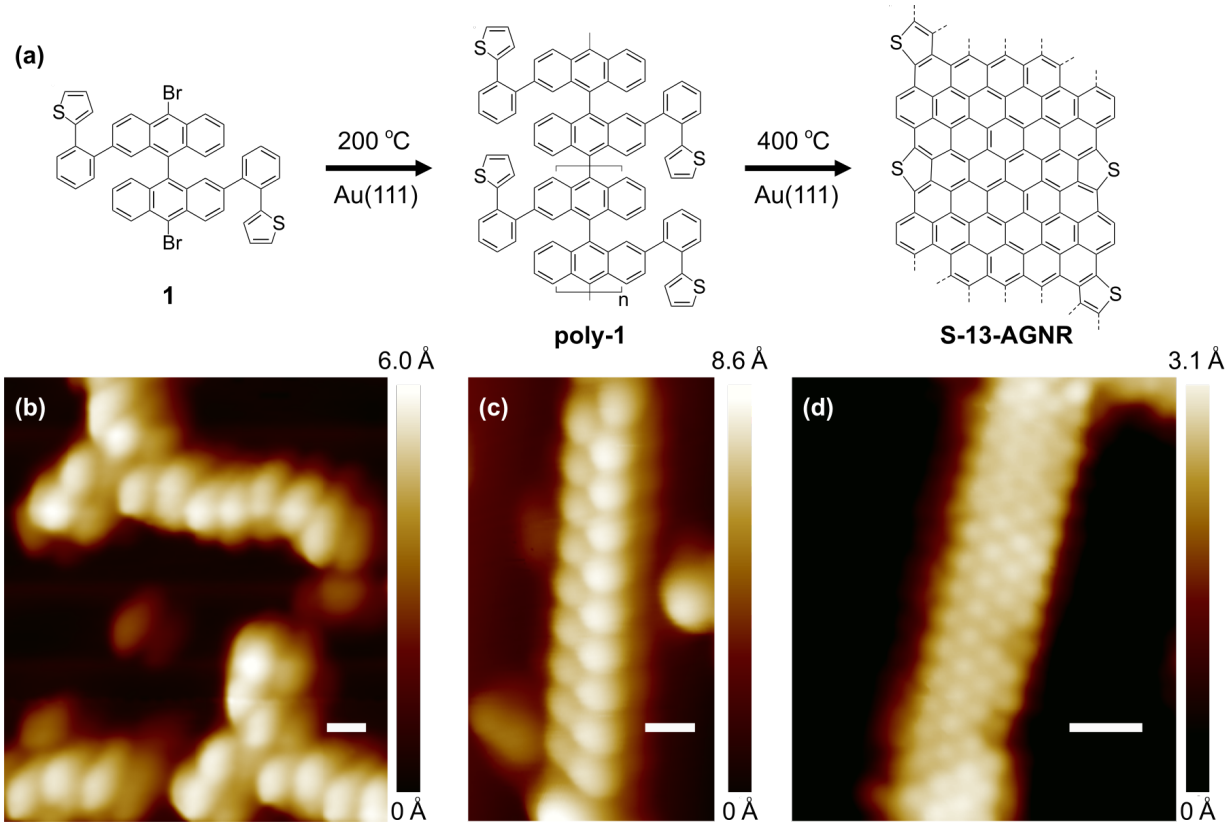

Figure 1. (a) Reaction scheme for bottom-up synthesis of S-13-AGNRs. Annealing at 200 °C induces radical step-growth polymerization. Annealing at 400 °C induces cyclodehydrogenation to yield S-13-AGNRs. (b) STM image of precursor **1** as deposited onto a Au(111) surface (V_s = 2.0 V, I_t = 20 pA, T = 13 K). (c) STM image of a *poly*-**1** (after first annealing step) shows characteristic pattern of alternating protrusions (V_s = 2.0 V, I_t = 20 pA, T = 13 K). (d) STM image of a fully cyclized S-13-AGNR (V_s = 0.1 V, I_t = 15 pA, T = 7 K). Scale bars are 1 nm.

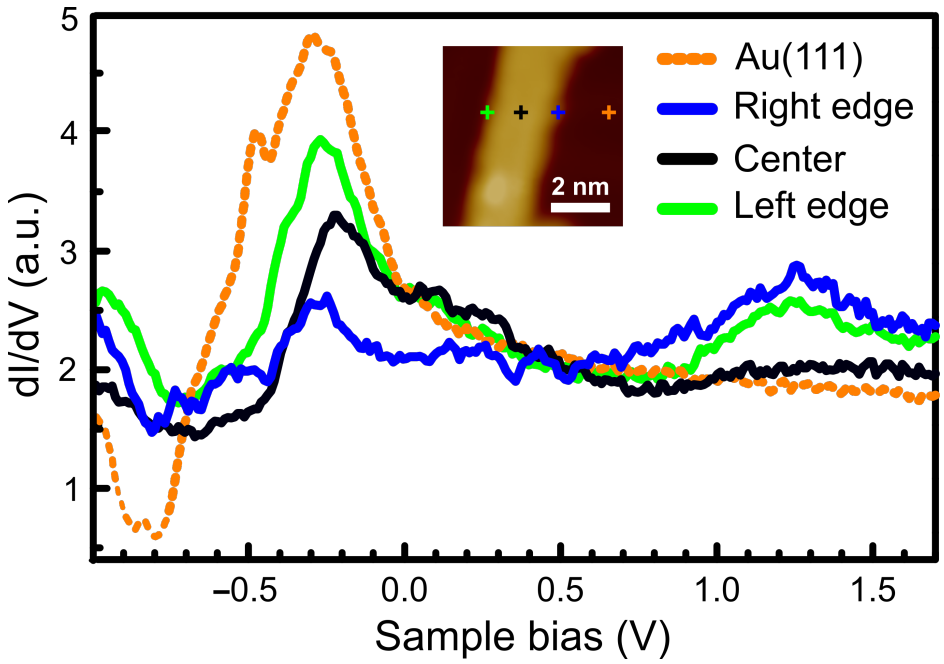

Figure 2. d*I*/d*V* spectra of S-13-AGNRs at different spatial positions compared to reference spectrum obtained on bare Au(111). Crosses in topographic STM image (inset) indicate the positions of recorded spectra (T =13 K).

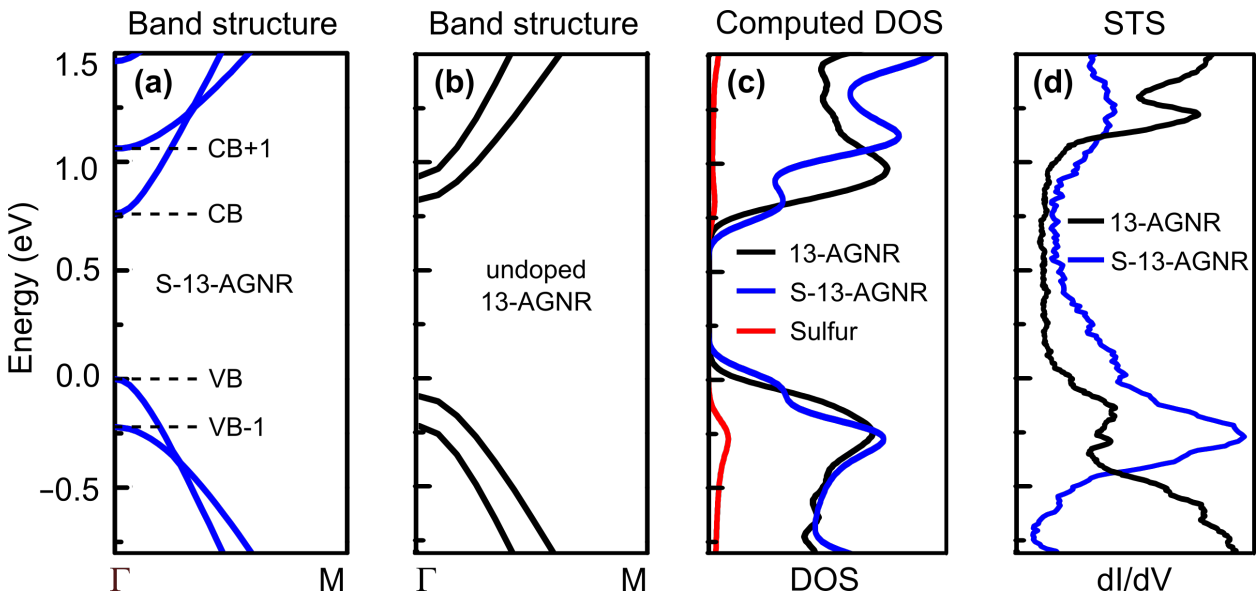

Figure 3. Computed band structures of (a) an S-13-AGNR and (b) a pristine 13-AGNR. (c) Calculated density of states (DOS) of an S-13-AGNR (blue), as well as the partial density of states (PDOS) of sulfur orbitals (red), and the DOS of a pristine 13-AGNR (black). (d) Experimental d*I*/d*V* spectrum for an S-13-AGNR (blue) compared to the d*I*/d*V* spectrum for a pristine 13-AGNR (black).

TOC figure